

# A Location-Dependent Base Station Cooperation Scheme for Cellular Networks

Ke Feng, *Student Member, IEEE*, and Martin Haenggi, *Fellow, IEEE*

**Abstract**—The link quality in cellular networks strongly depends on the location of the users relative to the serving and interfering base stations (BSs). This paper proposes a location-dependent BS cooperation scheme for general cellular networks, where BSs are modeled using a stationary point process and the Voronoi diagram forms the cell structure. The cooperation scheme is based on the relative average received signal strength from the three strongest BSs. For the channel model where Rayleigh fading and power-law path loss are considered, each cell is partitioned into three regions based on the relative distance to the three nearest BSs: the cell center region, cell edge region, and cell corner region. The area fraction of each region is tuned by the so-called cooperation level  $\gamma \in [0, 1]$ . We study the scheme where users in the above regions receive the non-coherent joint transmission from one, two, and three nearest BSs, respectively. As such, the scheme primarily helps users vulnerable to interference. We analyze the signal-to-interference ratio (SIR) in Poisson networks and show that a moderate  $\gamma$  jointly improves the average SIR performance and the network fairness.

**Index Terms**—Cellular networks, CoMP, base station cooperation, Poisson point process, stochastic geometry, meta distribution.

## I. INTRODUCTION

### A. Motivation

The link quality in cellular networks strongly depends on the location of the users relative to the serving and interfering BSs. In interference-limited networks, the signal-to-interference-ratio (SIR) averaged over small-scale fading varies from user to user depending on their geometric locations. Such a variation induces unfairness, and users near the cell boundary are known to be the bottleneck of the network performance [2]–[4]. BS cooperation, known as coordinated multipoint (CoMP) in 3GPP, is a technique to mitigate/exploit interference by coordinating the signal transmission or enabling the joint transmission/processing among a set of BSs. The design, analysis and optimization of BS cooperation schemes are of significant importance, as the gain of coordination comes at the cost of the backhaul capacity, channel state information (CSI), synchronization efforts, and, in general, more signaling overhead [5], [6].

BS cooperation primarily alleviates the signal degradation due to interference, thus users who are more vulnerable to interference should be prioritized for receiving cooperation over the average user; the size of cooperating set should be

limited for practical systems to balance the cost of data exchange through backhaul, signalling overhead, synchronization efforts, and number of BS resources per user. Thus, it is crucial to exploit cooperation schemes that allocate extra resources only to users who need them while limiting the number of cooperating BSs for each user. In this paper, we focus on a user-centric BS cooperation scheme with non-coherent joint transmission, where users are grouped by their relative received signal strengths to three strongest BSs and up to three BSs are turned into a set of cooperating BSs that jointly serve users without stringent requirement for implementation.

### B. Related Work

BS cooperation schemes mainly focuses on four aspects: the dependence of cooperation on users' channel (user-centric or not), the selection of the set of cooperating BSs (fixed-size or adaptive), the cooperation mode (BS silencing, point selection, coherent/non-coherent joint transmission), and its implementation challenges (limited backhaul, imperfect synchronization, imperfect CSI). [7]–[9] study user-centric BS cooperation while [10], [11] study BS cooperation where all users are non-coherently served by  $n$  strongest BSs. It is shown in [10] that users located at the Voronoi vertices benefit more from cooperation than the typical user. Also, it is shown in [11] that increasing the size of the cooperation set leads to a larger variance of the link success probability and thus reduces fairness. In [7], [8], the authors define the “cooperation region” such that users receive cooperation only when they are located in the cooperation region. Both definitions are based on the relative distances to the serving and the nearest interfering BS, and different cooperation modes are analyzed. In [7], BS silencing is activated for users in the cooperation region. However, it assumes a small-cell scenario where there are many inactive BSs and is thus less interference-limited. [8] studies the network where all BSs are always active. Users within the cooperation region are coherently served by the two nearest BSs. The scheme, however, relies on the precise channel phase match within the cooperating BSs. A transmission scheme that is less sensitive to channel estimation is analyzed in [9], where the cooperating BSs non-coherently transmit to the target user without exchanging CSI. The set of cooperating BSs is defined to be BSs within a disk of a fixed radius centered at each user. The definition depends on the selection of the radius and leads to an indefinite size of the cooperating set, which can boost the system complexity.

BS cooperation in a two-tier network is studied in [12], where the strongest BSs from each tier jointly serve users who

Part of this work has been presented at [1]. The work was supported by the U.S. NSF (grant CCF 1525904).

Ke Feng and Martin Haenggi are with the Department of Electrical Engineering, University of Notre Dame, Notre Dame, IN 46556 USA (e-mail: kfeng1@nd.edu; mhaenggi@nd.edu).

suffer from strong interference. The scheme does not consider the case when both the strongest serving BS and strongest interfering BS belong to the same tier.

### C. Contributions

In this paper, we study a location-dependent BS cooperation scheme that primarily helps users vulnerable to interference. Specifically, a user receives the non-coherent joint transmission from its one, two, or three strongest BSs depending on the user's geometrical region. The reason to focus on a maximum of three cooperating BSs is two-fold: (1) the size of cooperating BSs should be limited for practical implementation; (2) from a geometric point of view, a worst-case user lying on the Voronoi vertex has exactly three equidistant nearest BSs almost surely for most stationary point processes in  $\mathbb{R}^2$  (excluding lattices).

Throughout the paper, we assume all BSs are always active. Each uses the full frequency band and serves users with orthogonal resource blocks (RBs). The main contributions are:

- We mathematically define the cell center region, cell edge region, and cell corner region for any stationary BS point process in  $\mathbb{R}^2$  based on the relative distances of the three nearest BSs. While this paper focuses on Rayleigh fading and power-law path loss, the user grouping method is based on the relative average received signal strength from the three strongest BSs, which applies to general channel models and heterogeneous networks.
- We study a location-dependent BS cooperation scheme where users in the cell center region, cell edge region, and cell corner region are jointly served by one, two, and three nearest BSs, respectively. The area fraction of each region is tuned by a parameter  $\gamma$  that varies continuously from 0 to 1. The scheme permits the analysis of BS cooperation for different cooperation levels and the optimization of  $\gamma$  under practical system constraints.
- Both one-dimensional (1D) and two-dimensional (2D) Poisson networks are studied. It is worth noting that the analysis for Poisson networks applies to general networks with shadowing, as the large-scale path loss values (including shadowing) in all stationary models converge to those in Poisson networks as the shadowing variance increases [13]. We obtain analytical expressions for the success probability, and, more generally, the moments of the individual link success probability. We give the analytical form of the asymptotic SIR gain  $G$  and show that the asymptotic SIR gain increases with the path loss exponent  $\alpha$ .
- We study the spectral efficiency normalized by the number of cooperating BSs. The normalization permits the evaluation of BS cooperation gain without increasing the cell load, *i.e.*, users who receive cooperation from  $N$  BSs are served by  $1/N$  RBs from each BS. We show that with a moderate  $\gamma$ , the non-coherent joint transmission can improve users' throughput even with the normalization.
- We apply the methodology to general multi-tier networks, where the power and distance of the BSs are jointly considered in the user grouping. The homogeneous in-

TABLE I: Summary of Notation

Notation	Definition/Meaning
$\Phi; \lambda$	BS point process $\Phi$ with intensity $\lambda$
$\ \cdot\ $	Euclidean metric
$\gamma$	Cooperation level
$x_i(u)$	$i$ -th nearest BS to $u$
$\mathcal{C}_1$	Cell center region
$\mathcal{C}_2$	Cell edge region
$\mathcal{C}_3$	Cell corner region
$\mathcal{S}$	Set of cooperating BSs
$N$	Size of the cooperation set
$\alpha$	Path loss exponent
$\mathbb{1}(\cdot)$	Indicator function
$G$	Asymptotic SIR gain
$R$	Normalized spectral efficiency
$K$	Number of BS tiers
$\Phi_i; \lambda_i$	$i$ -th tier BS point process $\Phi_i$ with intensity $\lambda_i$
$P_i$	Power of the $i$ -th tier BSs

dependent Poisson (HIP) network is studied as a special case.

- We compare the asymptotic SIR gain in lattice networks (via simulation) to that in Poisson networks. The comparison shows that the asymptotic SIR gain as a function of  $\gamma$  behaves similarly across different types of networks.

### D. Organization of Paper

This paper is organized as follows. In Section II, we introduce the system model, the definition of the cell regions and the cooperation set. Both 1D and 2D network models are presented. Section III introduces the performance metrics of interest. Section IV studies the cooperation scheme for 1D Poisson networks, Section V for 2D Poisson networks and Section VI for 2D lattice networks. In Section VII, we provide a generalization of the cell regions to heterogeneous networks. Section VIII concludes our work. A summary of the notation can be found in Table I.

## II. SYSTEM MODEL AND COOPERATION SCHEME

In this section, we introduce our system model and define the cell regions under the considered model. The 1D case is presented first to obtain crisp insights for 2D networks.

### A. System Model

We focus on non-coherent joint transmission scheme to minimize the constraints on CSI. Let  $\Phi$  be any stationary point process modelling the geometric location of BSs. We consider iid Rayleigh fading and power-law path loss. The desired signals come from the set of cooperating BSs, denoted as  $\mathcal{S}$ , and the interference comes from the other BSs  $\Phi \setminus \mathcal{S}$ . The SIR of the typical user at the origin  $o$  is defined as

$$\text{SIR} \triangleq \frac{\left| \sum_{x \in \mathcal{S}} h_x \|x\|^{-\alpha/2} \right|^2}{\sum_{x \in \Phi \setminus \mathcal{S}} |h_x|^2 \|x\|^{-\alpha}}.$$

Here,  $(h_x)_{x \in \Phi}$  are iid complex Gaussian random variables modelling Rayleigh fading, and  $\alpha$  denotes the power-law path

loss exponent.  $g_x \triangleq |h_x|^2$  denotes the fading power that is exponentially distributed with unit mean.

The average received signal strength (over small-scale fading) at a user from each BS depends on the geometric distance. The SIR thus strongly depends on the relative distance(s) to the serving BS and the nearest interfering BS(s). In the Voronoi diagram of a BS point process  $\Phi \subset \mathbb{R}^2$ , locations on cell edges are equidistant to the two nearest BSs, and Voronoi vertices are equidistant to the three nearest BSs. As a result, users near the Voronoi edge suffer from relatively strong interference from one nearby BS, and users near the Voronoi vertices suffer from relatively strong interference from two nearby BSs. In the next subsection, we define the cell regions based on this observation.

### B. Cell Regions and Cooperation Set

1) *1D Networks*: The study of 1D networks serves as an interesting study in itself, *e.g.*, for modeling roadside BS deployments [14]. Its analysis also leads to insights that apply to 2D networks. For any stationary point process  $\Phi \subset \mathbb{R}$ , let  $x_i(u) \in \Phi$  be the  $i$ -th nearest BS to  $u$ . We denote by  $\mathcal{C}_1$  and  $\mathcal{C}_2$  the “cell center region” and the “cell edge region” respectively. For  $\gamma \in [0, 1]$  and  $\rho = 1 - \gamma$  we define

$$\begin{aligned} \mathcal{C}_1 &\triangleq \{u \in \mathbb{R}: \|u - x_1(u)\| \leq \rho \|u - x_2(u)\|\} \\ \mathcal{C}_2 &\triangleq \{u \in \mathbb{R}: \rho \|u - x_2(u)\| < \|u - x_1(u)\|\}. \end{aligned} \quad (1)$$

Note that  $\gamma = 0$  results in  $\mathcal{C}_1 = \mathbb{R}^2$  and  $\gamma = 1$  results in  $\mathcal{C}_2 = \mathbb{R}^2 \setminus \Phi$ .

We define the cooperation set  $\mathcal{S}$  to be

$$\mathcal{S} \triangleq \begin{cases} \{x_1(u)\}, & u \in \mathcal{C}_1 \\ \{x_1(u), x_2(u)\}, & u \in \mathcal{C}_2. \end{cases} \quad (2)$$

In words, a user in  $\mathcal{C}_i$  is jointly served by  $i$  BS(s) since it receives relatively strong signal(s) from  $i$  BS(s).  $\gamma$  is referred to as “the cooperation level” since the area fraction of  $\mathcal{C}_2$  increases monotonically with  $\gamma$ . This BS clustering method is simple yet effective, since in 1D networks, a worst-case user lying on the Voronoi vertex is equidistant to two nearest BSs almost surely. This intuition can be generalized to networks of arbitrary dimensions.

2) *2D Networks*: We now give a mathematical definition of the cell center region, the cell edge region, and the cell corner region in 2D networks based on the relative distances of the three nearest BSs. With a slight abuse of notation, we denote the regions as  $\mathcal{C}_1$ ,  $\mathcal{C}_2$ , and  $\mathcal{C}_3$ , respectively. For any stationary point process  $\Phi \subset \mathbb{R}^2$ , let  $x_i(u) \in \Phi$  denote the  $i$ -th nearest BS in the point process to  $u$ . For  $\gamma \in [0, 1]$  and  $\rho = 1 - \gamma$  we define

$$\begin{aligned} \mathcal{C}_1 &\triangleq \{u \in \mathbb{R}^2: \|u - x_1(u)\| \leq \rho \|u - x_2(u)\|\} \\ \mathcal{C}_2 &\triangleq \{u \in \mathbb{R}^2: \rho \|u - x_2(u)\| < \|u - x_1(u)\|, \\ &\quad \|u - x_1(u)\| \leq \rho \|u - x_3(u)\|\} \\ \mathcal{C}_3 &\triangleq \{u \in \mathbb{R}^2: \|u - x_1(u)\| > \rho \|u - x_3(u)\|\}. \end{aligned} \quad (3)$$

By definition, the area fraction of each region depends on  $\Phi$  and  $\gamma$ . Fig. 1 shows the partition for a realization of the Poisson point process (PPP). The cell corner region expands

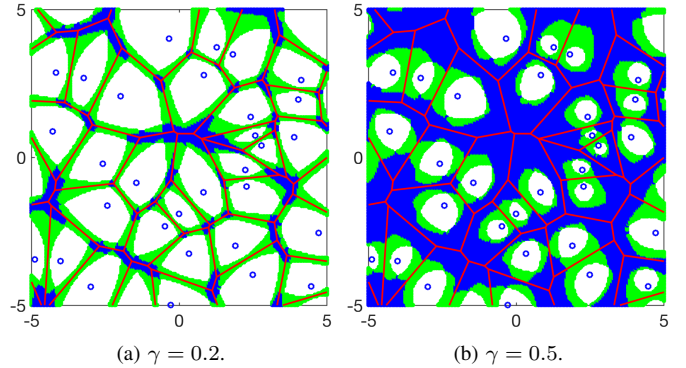


Fig. 1. Illustration of the partition for  $\gamma = 0.2$  and  $\gamma = 0.5$ . The location of the BSs (blue circles) is a realization of the PPP with intensity  $\lambda = 1$ . The window is  $[-5, 5]^2$ . Red lines are the edges of the Voronoi cells. Blank, green and blue regions denote the cell center region  $\mathcal{C}_1$ , the cell edge region  $\mathcal{C}_2$ , and the cell corner region  $\mathcal{C}_3$ , respectively.

and the cell center region shrinks as  $\gamma$  increases from 0.2 to 0.5. The boundaries of each region  $\mathcal{C}_i$  are formed by the union of circular arcs, where for each arc, the two nearest points of  $\Phi$  are the same and their distance ratio to a point of the arc is  $\rho$ .

We define the cooperation set  $\mathcal{S}$  to be

$$\mathcal{S} \triangleq \begin{cases} \{x_1(u)\}, & u \in \mathcal{C}_1 \\ \{x_1(u), x_2(u)\}, & u \in \mathcal{C}_2 \\ \{x_1(u), x_2(u), x_3(u)\}, & u \in \mathcal{C}_3. \end{cases} \quad (4)$$

In words, a user in  $\mathcal{C}_i$  is jointly served by  $i$  BS(s) since it receives relatively strong signal(s) from  $i$  BS(s). A worst-case user—a user lying on the Voronoi vertex—has exactly three equidistant nearest BSs almost surely for most stationary point processes in  $\mathbb{R}^2$ .

Note that  $\gamma = 0$  results in  $\mathcal{C}_1 = \mathbb{R}^2$  (no cooperation), and  $\gamma = 1$  results in  $\mathcal{C}_3 = \mathbb{R}^2 \setminus \Phi$  (full cooperation). The special cases  $\gamma \in \{0, 1\}$  for Poisson networks have been analyzed in [15], [16] and [10], [11], respectively.

## III. PERFORMANCE METRICS

### A. Success Probability

For a given threshold  $\theta$ , the success probability is defined as

$$\bar{F}(\theta) \triangleq \mathbb{P}(\text{SIR} > \theta), \quad (5)$$

which is the complementary cumulative distribution function (CCDF) of the SIR.

The success probability for the homogeneous PPP with intensity  $\lambda$  is

$$\bar{F}_{\text{PPP}}(\theta) = \frac{1}{{}_2F_1(1, -\delta; 1 - \delta; -\theta)}, \quad (6)$$

where  $\delta = d/\alpha$  and  $d$  is the dimension of the PPP. (6) has been derived for  $d = 2$  [15], [17] but can be shown to hold for Poisson networks of an arbitrary dimension.

### B. Asymptotic SIR Gain

While the success probability of all but a few basic network models is intractable, the asymptotic SIR gain [18] gives a simple and unified characterization of the SIR improvement compared to a baseline scheme. We use  $\bar{F}_{\text{PPP}}(\theta)$  given in (6) as our baseline model.  $\bar{F}_\gamma(\theta)$  denotes the success probability of our scheme with the cooperation level  $\gamma$ . We have

$$1 - \bar{F}_\gamma(\theta) \sim 1 - \bar{F}_{\text{PPP}}(\theta/G), \quad \theta \rightarrow 0, \quad (7)$$

where  $G$  denotes the asymptotic SIR gain and can be expressed as

$$G = \frac{\text{MISR}_{\text{PPP}}}{\text{MISR}_\gamma}. \quad (8)$$

The mean-interference-signal-ratio (MISR) [18]  $\text{MISR} \triangleq \mathbb{E}(I/\bar{S})$  is the ratio between the interference power  $I$  and the signal power averaged over the fading  $\bar{S} \triangleq \mathbb{E}_h(S)$ .  $\text{MISR}_{\text{PPP}}$  denotes the MISR of the baseline PPP model while  $\text{MISR}_\gamma$  denotes the MISR of our cooperation scheme with the cooperation level  $\gamma$ .

### C. SIR Meta Distribution

While the standard success probability characterizes the probability that the SIR of the typical link is greater than the threshold  $\theta$ , the SIR meta distribution [16] characterizes the fraction of individual links that achieve reliability  $x$  for a given threshold  $\theta$ . It answers questions such as “*what is the fraction of users in the network that achieve an SIR of 5 dB with probability 90%?*”, and is defined as

$$\bar{F}_{P_s}(x) \triangleq \mathbb{P}(P_s(\theta) > x), \quad x \in [0, 1], \quad (9)$$

which is the CCDF of the conditional success probability. The conditional success probability, also referred to as the individual link success probability, is defined as

$$P_s(\theta) \triangleq \mathbb{P}(\text{SIR} > \theta \mid \Phi), \quad (10)$$

which is the success probability given the point process  $\Phi$ .

The  $b$ -th moment of the conditional success probability is defined as

$$M_b(\theta) \triangleq \mathbb{E}(P_s(\theta)^b), \quad b \in \mathbb{C}. \quad (11)$$

Note that  $M_1(\theta) \equiv \bar{F}(\theta)$  is the standard success probability defined in (5).  $M_2(\theta) - M_1(\theta)^2$  is the variance of the individual link success probability, which measures the fairness of the individual link success probability across the network. We will mainly focus on the first two moments.

### D. Normalized Spectral Efficiency

The normalized spectral efficiency in units of nats/s/Hz/BS is defined as

$$R \triangleq \mathbb{E} \left[ \frac{1}{N} \log(1 + \text{SIR}) \right] \quad (12)$$

where  $N = |\mathcal{S}|$  is the size of cooperating BSs which depends on the region of the typical user. This normalization allows the evaluation of the benefits of cooperation while taking into account the number of RBs a user can occupy.

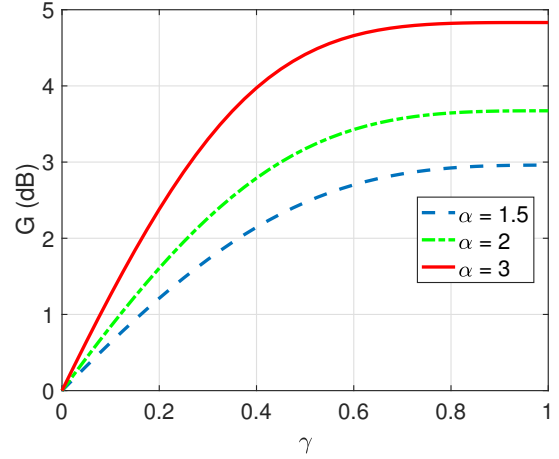


Fig. 2. The asymptotic SIR gain  $G$  (in dB) in 1D Poisson networks.

## IV. 1D POISSON NETWORKS

We first study the performance of the scheme in 1D Poisson networks, where  $\Phi \subset \mathbb{R}$  is a PPP with intensity  $\lambda$ . We focus on the typical user located at the origin. Let  $r_i = \|x_i(o)\|$  be the distance from the  $i$ -th nearest point to  $o$ ,  $h_i$  be the fading coefficient and  $g_i = |h_i|^2$  be the fading power. The joint distribution of  $r_1$  and  $r_2$  is

$$f_{r_1, r_2}(x, y) = (2\lambda\pi)^2 \exp(-2\lambda\pi y), \quad 0 \leq x \leq y. \quad (13)$$

The area fraction of each region only depends on  $\gamma$  and is equal to the probability that the origin falls into each region:

$$\mathbb{P}(o \in \mathcal{C}_1) = 1 - \gamma, \quad \mathbb{P}(o \in \mathcal{C}_2) = \gamma. \quad (14)$$

This follows from  $\mathbb{P}(o \in \mathcal{C}_1) = \int_0^\infty \int_{\frac{x}{\rho}}^\infty f_{r_1, r_2}(x, y) dy dx$  and  $\mathbb{P}(o \in \mathcal{C}_2) = \int_0^\infty \int_x^{\frac{x}{\rho}} f_{r_1, r_2}(x, y) dy dx$ . Note that due to the ergodicity of the PPP, the area fraction of each region is (14) for each realization of the BS point process.

### A. Asymptotic SIR Gain

We now study the asymptotic SIR gain  $G$  and show that  $G$  is a function only of  $\alpha$  and  $\gamma$ .

**Theorem 1.** The asymptotic SIR gain of the proposed BS cooperation scheme in 1D Poisson networks is

$$G = \left( \rho^{1+\alpha} + 2 \left( 1 - \rho - \int_\rho^1 \frac{1}{1+z^\alpha} dz \right) \right)^{-1}, \quad (15)$$

where  $\delta = 1/\alpha$ ,  $\delta < 1$ . For  $\alpha = 2$ ,

$$G^{-1} = \rho^3 + 2 \left( 1 - \rho - \frac{\pi}{4} + \arctan \rho \right), \quad (16)$$

and for  $\alpha = 4$ ,

$$G^{-1} = \rho^5 + 2(1 - \rho) + \frac{1}{2\sqrt{2}} \log \frac{1 + \rho^2 + \sqrt{2}\rho}{1 + \rho^2 - \sqrt{2}\rho} - \frac{1}{2\sqrt{2}} (\pi + \log(3 + 2\sqrt{2})) - \frac{1}{\sqrt{2}} \arctan \frac{\sqrt{2}\rho}{1 - \rho^2}. \quad (17)$$

*Proof.* See Appendix A.  $\square$

Fig. 2 shows the asymptotic SIR gain in 1D Poisson networks using (15). The curves suggest that the slope of  $G$  goes to 0 as  $\gamma$  approaches 1 regardless of  $\alpha$ . We now show that it is indeed the case.

**Corollary 1** (Derivative at  $\gamma = 0$  and  $\gamma = 1$ ). The asymptotic SIR gain  $G$  in 1D Poisson networks satisfies

$$\frac{\partial G}{\partial \gamma} \Big|_{\gamma=0} = \alpha, \quad \frac{\partial G}{\partial \gamma} \Big|_{\gamma=1} = 0. \quad (18)$$

*Proof.* By taking the derivative of  $G$  with respect of  $\rho$ , we obtain

$$\frac{\partial G}{\partial \rho} = -G^2 \left( \alpha + 1 - \frac{2}{1 + \rho^\alpha} \right) \rho^\alpha. \quad (19)$$

Setting  $\gamma = 0$  ( $\rho = 1$ ) we get  $G'|_{\gamma=0} = -G'|_{\rho=1} = \alpha$  and setting  $\gamma = 1$  ( $\rho = 0$ ) we get  $G'|_{\gamma=1} = -G'|_{\rho=0} = 0$ . This holds for any  $\alpha > 1$ .  $\square$

**Remark 1.** For any fixed  $\alpha$ ,  $G$  monotonically increases with the cooperation level  $\gamma$ . The slope at  $\gamma = 0$  is determined by the path loss exponent  $\alpha$  and is 0 at  $\gamma = 1$ . It can be shown that the second derivative is first positive and then negative, *i.e.*, the slope of  $G$  increases slightly beyond  $\alpha$  at the beginning before decreasing to 0.

For any fixed  $\gamma$ ,  $G$  monotonically increases with the path loss exponent  $\alpha$ . As a result, under the same cooperation level, users benefit more from cooperation when the signal decays faster with distance. The rationale is while both the desired signals and interference will decay faster with a larger  $\alpha$ , their ratio grows with  $\alpha$ . Nevertheless, there is a limit to the achievable gain, since the network becomes noise-limited at some point.

## B. SIR Meta Distribution

### 1) Conditional Success Probability:

**Lemma 1.** For the location-dependent cooperation scheme in general 1D networks, we have

$$P_s(\theta) = \begin{cases} \prod_{i=2}^{\infty} \frac{1}{1 + \theta r_i^{-\alpha}/r_1^{-\alpha}}, & o \in \mathcal{C}_1 \\ \prod_{i=3}^{\infty} \frac{1}{1 + \theta r_i^{-\alpha}/(r_1^{-\alpha} + r_2^{-\alpha})}, & o \in \mathcal{C}_2. \end{cases} \quad (20)$$

*Proof.* For  $o \in \mathcal{C}_1$ , the typical user is associated with the nearest BS only, hence

$$\begin{aligned} P_s(\theta) &= \mathbb{P} \left( g_1 r_1^{-\alpha} > \theta \sum_{i=2}^{\infty} g_i r_i^{-\alpha} \right) \\ &\stackrel{(a)}{=} \mathbb{E} \left[ \exp \left( -\theta \sum_{i=2}^{\infty} g_i r_i^{-\alpha} / r_1^{-\alpha} \right) \right] \\ &\stackrel{(b)}{=} \mathbb{E} \left[ \prod_{i=2}^{\infty} \exp(-\theta g_i r_i^{-\alpha} / r_1^{-\alpha}) \right] \\ &= \prod_{i=2}^{\infty} \frac{1}{1 + \theta r_i^{-\alpha} / r_1^{-\alpha}}. \end{aligned} \quad (21)$$

Step (a) follows the exponential distribution of the fading power. Step (b) follows from the independence of fading coefficients.

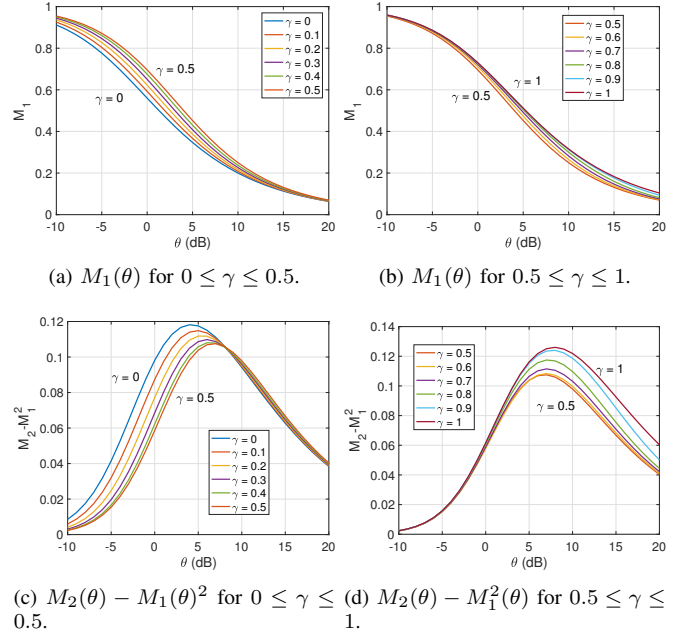


Fig. 3. The mean  $M_1(\theta)$  and variance  $M_2(\theta) - M_1(\theta)^2$ ,  $\alpha = 2$ .

For  $o \in \mathcal{C}_2$ , the typical user receives the non-coherent joint transmission from two nearest BSs, and thus

$$\begin{aligned} P_s(\theta) &= \mathbb{P} \left( |h_1 r_1^{-\alpha/2} + h_2 r_2^{-\alpha/2}|^2 > \theta \sum_{i=3}^{\infty} g_i r_i^{-\alpha} \right) \\ &\stackrel{(a)}{=} \mathbb{E} \left[ \prod_{i=3}^{\infty} \exp(-\theta g_i r_i^{-\alpha} / (r_1^{-\alpha} + r_2^{-\alpha})) \right] \\ &= \prod_{i=3}^{\infty} \frac{1}{1 + \theta r_i^{-\alpha} / (r_1^{-\alpha} + r_2^{-\alpha})}. \end{aligned} \quad (22)$$

Step (a) follows from the fact that  $|h_1 r_1^{-\alpha/2} + h_2 r_2^{-\alpha/2}|^2$  is exponentially distributed with mean  $r_1^{-\alpha} + r_2^{-\alpha}$ , and the fading coefficients are independent.  $\square$

### 2) Moments:

**Proposition 1.** The  $b$ -th moment of the conditional success probability of the proposed scheme in 1D Poisson networks is

$$\begin{aligned} M_b(\theta) &= \frac{\rho}{{}_2F_1(b, -\delta; 1 - \delta; -\rho^\alpha \theta)} \\ &\quad + \int_1^{\frac{1}{\rho}} \frac{1}{(t {}_2F_1(b, -\delta, 1 - \delta, -\theta/(1 + t^{\frac{1}{\delta}})))^2} dt. \end{aligned} \quad (23)$$

where  $b \in \mathbb{C}$  and  $\delta = 1/\alpha$ .

*Proof.* See Appendix B.  $\square$

We focus on the first two moments of  $P_s(\theta)$ . For  $b = 1$ ,  $M_1(\theta) \equiv \bar{F}_\gamma(\theta)$ , and we obtain the success probability

$$\begin{aligned} M_1(\theta) &= \frac{\rho}{{}_2F_1(1, -\delta; 1 - \delta; -\rho^\alpha \theta)} \\ &\quad + \int_1^{\frac{1}{\rho}} \frac{1}{(t {}_2F_1(1, -\delta, 1 - \delta, -\theta/(1 + t^{\frac{1}{\delta}})))^2} dt. \end{aligned} \quad (24)$$

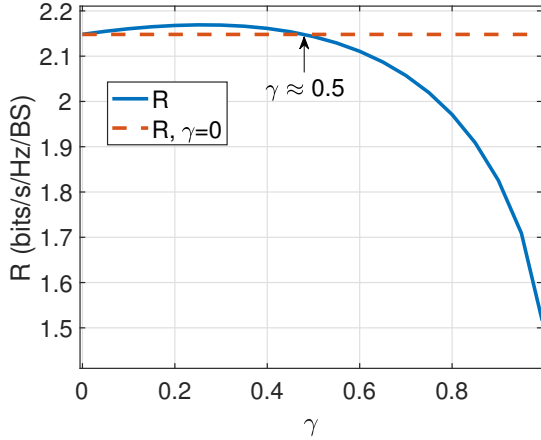


Fig. 4. The normalized spectral efficiency for  $\alpha = 2$  ( $\delta = 1/2$ ) per (27).

The success probability improves monotonically with  $\gamma$ . The two parts of the success probability correspond to the cases when the typical user is in the cell center region and when the typical user is in the cell edge region.  $M_2(\theta) - M_1(\theta)^2$  is the variance of the conditional success probability, reflecting the disparity in the link success probability. Ideally, the network is fairest when the link success probability is highly concentrated around the (mean) success probability. Thus, the variance of the conditional success probability serves as an insightful criterion of the network fairness.

The mean and variance of the conditional success probability for  $\delta = 1/2$  is shown in Fig. 3. The horizontal shift is less significant as  $\gamma$  increases, which is consistent with Fig. 2. In comparison, the maximal variance of the conditional success probability decreases first, achieves its minimal at  $\gamma \approx 0.5$  and then increases. For instance, at  $\theta = -5$  dB, as  $\gamma$  increases from 0 to 0.5, the success probability increases from 0.776 to 0.872, and the maximal variance decreases from 0.0415 to 0.0154. Hence, a moderate level of BS cooperation jointly improves the SIR performance and the fairness of the individual link quality.

### C. Normalized Spectral Efficiency

The average number of serving BSs per user is

$$\mathbb{E}N = 1 - \gamma + 2\gamma = 1 + \gamma. \quad (25)$$

The normalized spectral efficiency in units of nats/s/Hz/BS is

$$R = \int_0^\infty \mathbb{P}(\text{SIR} > e^t - 1, o \in C_1) dt + \frac{1}{2} \int_0^\infty \mathbb{P}(\text{SIR} > e^t - 1, o \in C_2) dt, \quad (26)$$

where  $\mathbb{P}(\text{SIR} > e^t - 1, o \in C_i)$ ,  $i = 1, 2$ , are given in (24). For  $\alpha = 2$ , we have

$$R = \int_0^\infty \frac{\rho}{1 + \rho\sqrt{e^x - 1} \arctan(\rho\sqrt{e^x - 1})} dx + \frac{1}{2} \int_0^\infty \int_1^{\frac{1}{\rho}} \frac{1}{t^2 (1 + \sqrt{\frac{e^x - 1}{1 + t^\alpha}} \arctan \sqrt{\frac{e^x - 1}{1 + t^\alpha}})^2} dt dx. \quad (27)$$

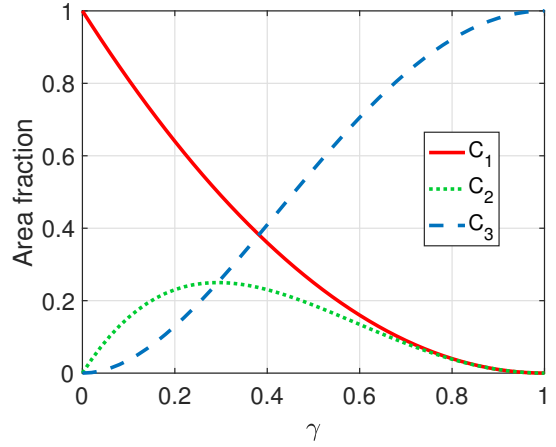


Fig. 5. The area fraction of the three regions.

Fig. 4 shows the normalized spectral efficiency as a function of  $\gamma$  per (27). The normalized spectral efficiency first increases and then decreases. The same value of  $R$  is achieved around  $\gamma = 0.5$  as in the non-cooperation case ( $\gamma = 0$ ) when  $\alpha = 2$ . Interestingly, the maximal variance also achieves minimum value at  $\gamma \approx 0.5$ .

## V. 2D POISSON NETWORKS

In this section, we study the performance of the scheme in 2D Poisson networks, where  $\Phi \subset \mathbb{R}^2$  is a PPP with intensity  $\lambda$ . The performance analysis has applicability beyond Poisson networks. In fact, the signal strengths for any stationary point process with shadowing converge in distribution to those in Poisson networks as the shadowing variance increases [13].

Let  $r_i = \|x_i(o)\|$  be the distance from the origin to its  $i$ -th nearest BS as defined before. The joint distribution of  $r_1, r_2$  and  $r_3$  is

$$f_{r_1, r_2, r_3}(x, y, z) = (2\lambda\pi)^3 xyz \exp(-\lambda\pi z^2), \quad 0 \leq x \leq y \leq z.$$

The area fraction of each region depends on  $\gamma$  and is equal to the probability that the origin falls into each region [17]:

$$\begin{aligned} \mathbb{P}(o \in C_1) &= (1 - \gamma)^2, \\ \mathbb{P}(o \in C_2) &= \gamma(1 - \gamma)^2(2 - \gamma), \\ \mathbb{P}(o \in C_3) &= \gamma^2(2 - \gamma)^2. \end{aligned} \quad (28)$$

Fig. 5 shows the area fraction of the three regions as  $\gamma$  increases from 0 to 1.

### A. Asymptotic SIR Gain

**Theorem 2.** The asymptotic SIR gain of the proposed BS cooperation scheme in 2D Poisson networks is (30) (see next page). For  $\alpha = 4$ , we have

$$G^{-1} = \rho^6 + \rho^8 \left( \frac{2}{\rho^2} - \frac{\pi}{2} + 2 \arctan \rho^2 - 2 \right) + 3 \int_0^\infty \int_x^{\frac{x}{\rho}} \int_{\frac{x}{\rho}}^\infty \frac{8xyz^{-3}e^{-z^2}}{x^{-4} + y^{-4} + z^{-4}} dz dy dx. \quad (29)$$

*Proof.* See Appendix C.  $\square$

$$G = \frac{2}{(\alpha + 2)\mathbb{E}\left[\left(\frac{r_1}{r_2}\right)^\alpha \mathbb{1}_{\mathcal{C}_1}\right] + (\alpha + 4)\mathbb{E}\left[\frac{(r_1/r_3)^\alpha}{1+(r_1/r_2)^\alpha} \mathbb{1}_{\mathcal{C}_2}\right] + 6\mathbb{E}\left[\frac{(r_1/r_3)^\alpha}{1+(r_1/r_2)^\alpha + (r_1/r_3)^\alpha} \mathbb{1}_{\mathcal{C}_3}\right]}. \quad (30)$$

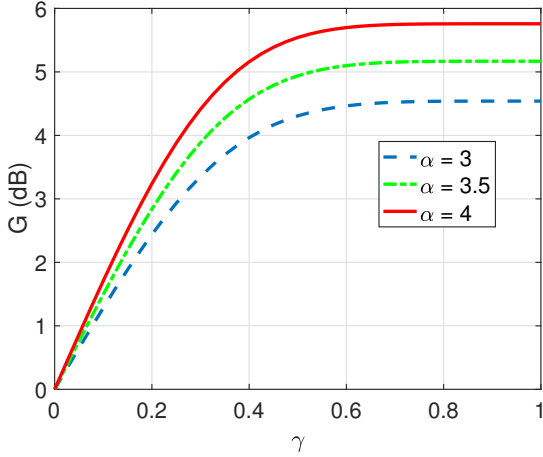


Fig. 6. The asymptotic SIR gain  $G$  (in dB) using (30).

Fig. 6 shows the asymptotic SIR gain as a function of  $\gamma$  for  $\alpha = 3, 3.5, 4$ . For any fixed  $\alpha$ , the asymptotic SIR gain increases with the cooperation level  $\gamma$ . For any fixed  $\gamma$ , the asymptotic SIR gain increases with the path loss exponent  $\alpha$ . When the path loss exponent  $\alpha$  grows larger than 4, the transmission scenario eventually approaches the point-to-point transmission scenario where the interference is negligible—the interference-free scenario. In this case, the network is no longer interference-limited and the effect of noise needs to be considered.

We observe a similar pattern of  $G$  in terms of its slope as in 1D Poisson networks. We now study its derivative in 2D Poisson networks.

**Corollary 2** (Derivative at  $\gamma = 0$  and  $\gamma = 1$ ). The asymptotic SIR gain  $G$  in 2D Poisson networks satisfies

$$\left. \frac{\partial G}{\partial \gamma} \right|_{\gamma=0} = \alpha, \quad \left. \frac{\partial G}{\partial \gamma} \right|_{\gamma=1} = 0. \quad (31)$$

*Proof.* The proof is straightforward and parallel to the proof for Corollary 1.  $\square$

### B. SIR Meta Distribution

1) *Conditional Success Probability:* Similar to Lemma 1, the conditional success probability for the cooperation scheme in general 2D networks can be written as

$$P_s(\theta) = \begin{cases} \prod_{i=2}^{\infty} \frac{1}{1+\theta r_i^{-\alpha}/r_1^{-\alpha}}, & o \in \mathcal{C}_1 \\ \prod_{i=3}^{\infty} \frac{1}{1+\theta r_i^{-\alpha}/\sum_{k=1}^2 r_k^{-\alpha}}, & o \in \mathcal{C}_2 \\ \prod_{i=4}^{\infty} \frac{1}{1+\theta r_i^{-\alpha}/\sum_{k=1}^3 r_k^{-\alpha}}, & o \in \mathcal{C}_3. \end{cases} \quad (32)$$

#### 2) Moments:

**Proposition 2.** The  $b$ -th moment of the conditional success probability of the proposed scheme in 2D Poisson networks is (33) (see next page) where  $F_b(x) = {}_2F_1(b, -\delta; 1 - \delta; -\frac{\theta}{x})$ .

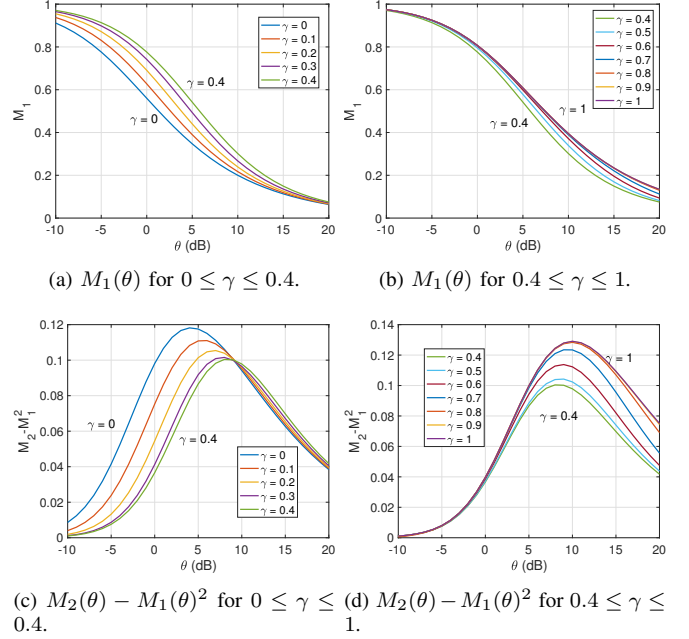


Fig. 7. The mean  $M_1(\theta)$  and variance  $M_2(\theta) - M_1(\theta)^2$ ,  $\alpha = 4$ .

*Proof.* The proof is parallel to the proof for Proposition 1 in Appendix B and thus omitted.  $\square$

To evaluate the average SIR performance and the network fairness, we focus on the mean and variance of  $P_s(\theta)$ . Fig. 7 shows the mean and variance of the conditional success probability as a function of  $\theta$  from  $\gamma = 0$  to  $\gamma = 1$ .

**Remark 2.** For  $0 \leq \gamma \leq 0.4$ , the maximal variance is monotonically decreasing. For  $\gamma > 0.4$ , the maximal variance starts to increase monotonically. So the minimal maximal variance is achieved when  $\gamma \approx 0.4$ . For  $0 \leq \gamma \leq 0.4$ , the variance when  $\theta > 10$  dB is essentially the same. For  $\gamma > 0.4$ , the variance when  $\theta < 0$  dB is essentially the same. In contrast to our user-centric scheme, [11] studies the scheme where all users are jointly served by the same number of BSs. It is shown that the maximum variance monotonically increases with the number of cooperating BSs. Essentially, user-centric BS cooperation can improve fairness by primarily helping users with bad locations.

**Remark 3.** For small  $\theta$ , the main reason not to succeed is bad fading (fading defines the asymptotic slope of the success probability as  $\theta \rightarrow 0$ ). The secondary reason is bad location. Cooperation helps with both, but it makes less of a difference for users in a good location—users near the cell center almost all succeed anyway, even without cooperation. Hence for small  $\theta$ ,  $M_1(\theta)$  does not change anymore once  $\gamma > 0.4$ . Similarly, for the variance, all users who need help are receiving it at  $\gamma < 0.4$ . For larger  $\gamma$ , there is a negligible improvement for most users, hence no further reduction in variance.

$$M_b(\theta) = \frac{\rho^2}{{}_2F_1(b, -\delta; 1-\delta, -\rho^\alpha \theta)} + \int_0^\infty \int_x^{\frac{x}{\rho^2}} \int_{\frac{x}{\rho^2}}^\infty \exp\left(-zF_b\left(\left(\frac{z}{x}\right)^{\frac{1}{\delta}} + \left(\frac{z}{y}\right)^{\frac{1}{\delta}}\right)\right) \left(1 + \frac{\theta}{\left(\frac{z}{y}\right)^{\frac{1}{\delta}} + \left(\frac{z}{x}\right)^{\frac{1}{\delta}}}\right)^{-b} dz dy dx$$

$$+ \int_0^\infty \int_x^{\frac{x}{\rho^2}} \int_y^{\frac{x}{\rho^2}} \exp\left(-zF_b\left(1 + \left(\frac{z}{x}\right)^{\frac{1}{\delta}} + \left(\frac{z}{y}\right)^{\frac{1}{\delta}}\right)\right) dz dy dx, \quad b \in \mathbb{C},$$
(33)

For large  $\theta$ , the main reason to succeed is good location (proximity to the serving BS defines the asymptotic slope as  $\theta \rightarrow \infty$ ). Users who are quite close to their BS but not extremely close will benefit from cooperation, which means that  $\gamma$  needs to be fairly large ( $> 0.4$ ) to make a difference in  $M_1(\theta)$ . Conversely, users who get cooperation for  $\gamma < 0.4$  are in such bad location that they cannot succeed at high  $\theta$ . Similarly, for the variance, for  $\gamma < 0.4$  there is no impact since no user switches from not succeeding to succeeding. For  $\gamma > 0.4$ , the users in almost-great locations start to benefit from cooperation (while those in bad locations still do not), which widens the gap between the two, increasing the variance. This is the regime where “the rich get richer”.

3) *SIR Meta Distribution*: The meta distribution is the distribution of the conditional success probability, which is hard to calculate in general. The moments of the conditional success probability is easier to calculate using the PGFL of the PPP. Recently, [19] and [20] propose two approximations of the SIR meta distribution, based on strategies to retrieve the distribution of a random variable with bounded support given its moments (known as the Hausdorff moment problem). In [16], an approximation of the meta distribution by matching its first two moments to beta distribution is proposed, which is quite accurate. We use this method here due to its simplicity. It yields

$$\bar{F}_{P_s}(\theta, x) \approx 1 - I_x\left(\frac{M_1\beta}{1-M_1}, \beta\right) \quad (34)$$

with

$$I_x(a, b) = \frac{\int_0^x t^{a-1}(1-t)^{b-1} dt}{B(a, b)} \quad (35)$$

and

$$\beta = \frac{(M_1 - M_2)(1 - M_1)}{M_2 - M_1^2}. \quad (36)$$

Using (34), we obtain the following plots of the meta distribution.

Fig. 8 shows the meta distribution as a function of the reliability, with fixed  $\theta = -10, 5, 0, 5$  dB. Observe that the gap between adjacent curves (with  $\gamma$  changed by 0.1) gets smaller as  $\gamma$  increases. Fig. 9 shows a contour plot of the SIR meta distribution for different  $\gamma$  when  $\bar{F}_{P_s}(\theta, x) = 0.95$  (i.e., 95% of the user in the network achieves reliability above  $x$  for the SIR threshold  $\theta$ ). Observe the trade-off between the reliability and the SIR threshold when the user percentage is fixed. For  $\theta \leq 0$  dB, the reliability improves significantly, as the cooperation scheme primarily helps users to succeed with small  $\theta$ . The improvement from  $\gamma = 0.4$  to  $\gamma = 0.5$  is barely noticeable.

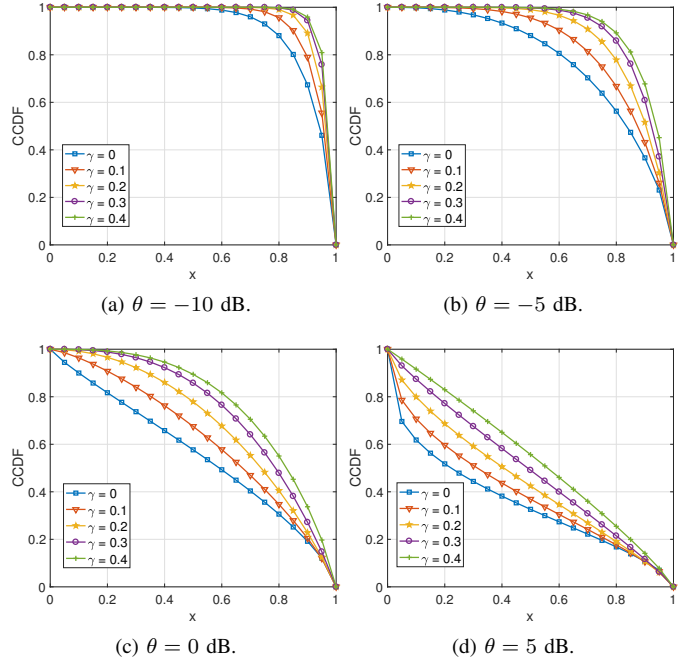


Fig. 8. The meta distribution  $\bar{F}_{P_s}(\theta, x)$  for  $\theta = -10, -5, 0, 5$  dB,  $\alpha = 4$ .

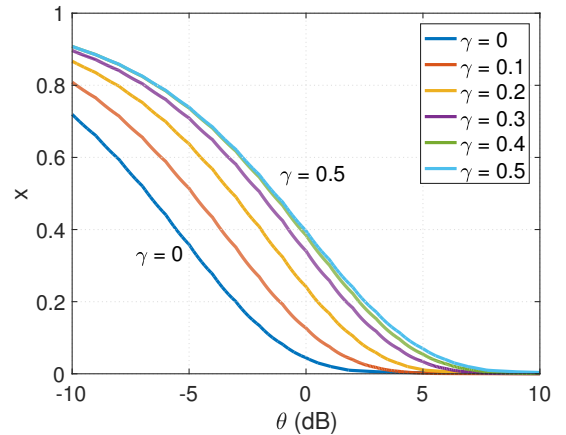


Fig. 9. The performance of the “5% user”,  $\alpha = 4$ .

### C. Normalized Spectral Efficiency

The normalized spectral efficiency can be written analytically similar to (27) in Section IV-C. However, it involves complex multiple integrals, and we will show the simulation result instead. Fig. 10 shows our simulation result in a PPP network and evaluate the normalized spectral efficiency at the typical user for 100,000 realizations of the network. In each realization, BS locations are generated according to the PPP of unit intensity with a window of  $[-20, 20]^2$ . The normalized

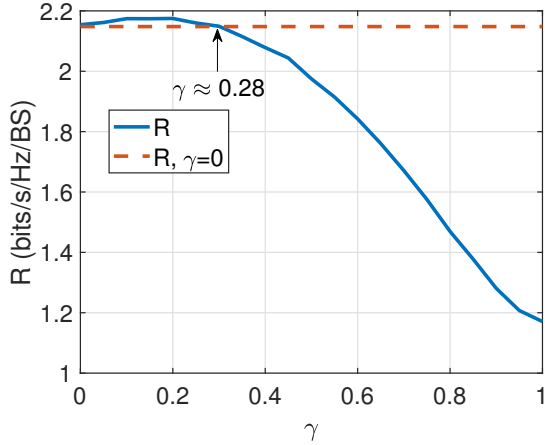


Fig. 10. The normalized spectral efficiency via simulation,  $\alpha = 4$ .

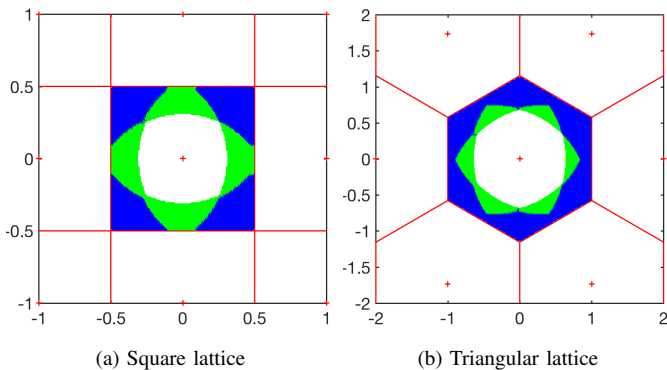


Fig. 11. The three regions in a square lattice and a triangular lattice network when  $\gamma = 0.5$ . Only one cell is colored since all cells are shifted version of each other. Red crosses and red lines denote the BSs and the edges of the associated Voronoi cells in the lattice. Blank, green and blue regions denote  $C_1$ ,  $C_2$  and  $C_3$  respectively.

spectral efficiency (in units of bits/s/Hz/BS) increases slightly and then decreases wrt  $\gamma$ . Observe that the same normalized spectral efficiency is achieved when  $\gamma = 0$  and  $\gamma \approx 0.28$ . As a result,  $\gamma \leq 0.28$  is the range of the cooperation level that improves the typical link quality without lowering the overall throughput. The optimum reliability performance is essentially achieved at  $\gamma \approx 0.4$ , where the normalized spectral efficiency is decreased by only about 3.4%.

## VI. LATTICE NETWORKS

In this section, we apply the scheme to two single-tier lattice networks, namely square lattice and triangular lattice networks. Lattice networks are generally less tractable but they provide upper bounds on the network performance due to the optimistic assumption of the BS deployment. Here, we confine our analysis to the asymptotic SIR gain and make a comparison between Poisson and lattice networks.

The area fraction of each region in a lattice network can be analytically calculated thanks to its rigid structure. The boundaries of each region  $C_i$  are formed by the union of circular arcs, where for each arc, the two nearest points of the lattice are the same and their distance ratio to a point of the arc is  $\rho$ . Note that all the arcs have the same radius and

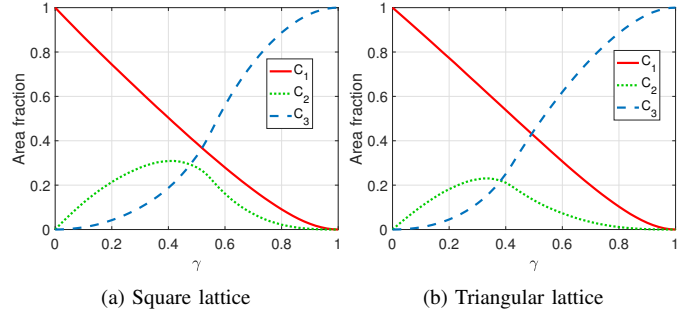


Fig. 12. The area fractions of the three regions for square and triangular lattices

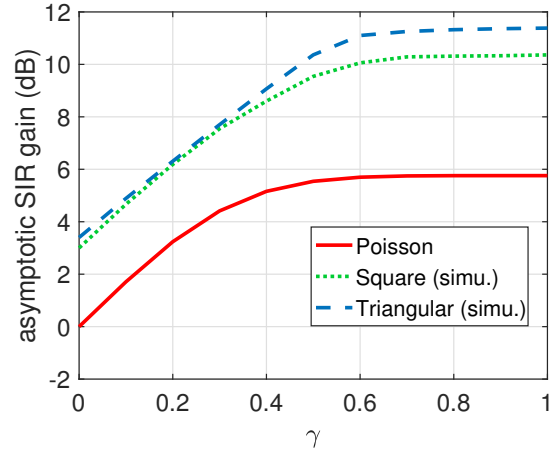


Fig. 13. The comparison of the asymptotic SIR gain in Poisson networks and lattice networks,  $\alpha = 4$ .

angle depending on  $\gamma$ , as shown in Fig. 11. Fig. 12 shows the area fraction of each region as  $\gamma$  increases from 0 to 1.

In the simulation, BSs are generated according to the lattice with unit intensity, with a window of  $[-20, 20]^2$ . The lattice is shifted such that the origin is in the center of a cell. The SIR is evaluated for 100,000 users placed uniformly at random in that cell. For each user, the fading coefficients from all BSs are generated independently according to complex Gaussian random variables. In Fig. 13, we compare the asymptotic SIR gain in Poisson networks and lattice networks. The asymptotic SIR gain in the lattice cases is approximated using the SIR shift of the success probability evaluated at  $\bar{F}_\gamma(\theta) = 0.95$ . The gap at  $\gamma = 0$  is the inherent SIR gain between Poisson and lattice networks (3 dB and 3.4 dB respectively for  $\alpha = 4$  [18]). All three curves increase almost linearly at the beginning and tend to saturate around  $\gamma = 0.6$ . The comparison reveals the similarity of the SIR gain of the proposed BS cooperation scheme in different networks.

## VII. MULTI-TIER NETWORKS

Multi-tier networks characterize BS deployment where BSs at different tiers have different transmission powers, spatial densities, maximum load, etc. We study a  $K$ -tier network  $\Phi = \bigcup_{i=1}^K \Phi_i$ , where the  $i$ -th tier is modelled using a stationary and ergodic point process  $\Phi_i \subset \mathbb{R}^2$ ,  $1 \leq i \leq K$ . Note that the dependence between BS tiers need not be specified. Our definition of the ‘‘cell regions’’ includes the power of each tier

to reflect the average received signal strengths.  $K = 1$  is the single-tier case where the regions are defined based on the distances only. We limit our partition to three regions with a maximum of three cooperating BSs being as before.

### A. Cell Regions and Cooperation Set

Assume BSs at the  $i$ -th tier transmits with power  $P_i$ ,  $1 \leq i \leq K$ . For a user at location  $u$ , let  $x_i(u)$  be its  $i$ -th strongest BS and  $v(x_i(u))$  be the index of the tier  $x_i(u)$  belongs to, *i.e.*,

$$x_i(u) \in \Phi_{v(x_i(u))}. \quad (37)$$

We have

$$\frac{\|x_i(u) - u\|}{P_{v(x_i(u))}^{1/\alpha}} \leq \frac{\|x_j(u) - u\|}{P_{v(x_j(u))}^{1/\alpha}}, \quad i \leq j. \quad (38)$$

Letting  $\rho = 1 - \gamma$  we define

$$\begin{aligned} \mathcal{C}_1 &\triangleq \left\{ u \in \mathbb{R}^2: \frac{\|x_1(u) - u\|}{P_{v(x_1(u))}^{1/\alpha}} \leq \rho \frac{\|x_2(u) - u\|}{P_{v(x_2(u))}^{1/\alpha}} \right\} \\ \mathcal{C}_2 &\triangleq \left\{ u \in \mathbb{R}^2: \rho \frac{\|x_2(u) - u\|}{P_{v(x_2(u))}^{1/\alpha}} < \frac{\|x_1(u) - u\|}{P_{v(x_1(u))}^{1/\alpha}}, \right. \\ &\quad \left. \frac{\|x_1(u) - u\|}{P_{v(x_1(u))}^{1/\alpha}} \leq \rho \frac{\|x_3(u) - u\|}{P_{v(x_3(u))}^{1/\alpha}} \right\} \\ \mathcal{C}_3 &\triangleq \left\{ u \in \mathbb{R}^2: \frac{\|x_1(u) - u\|}{P_{v(x_1(u))}^{1/\alpha}} > \rho \frac{\|x_3(u) - u\|}{P_{v(x_3(u))}^{1/\alpha}} \right\}. \end{aligned} \quad (39)$$

For a cooperation level  $\gamma$  we partition the plane into three regions based on the relative average received signal strengths from the three strongest BSs.  $\mathcal{C}_1$ ,  $\mathcal{C}_2$ , and  $\mathcal{C}_3$  are referred to as the ‘‘cell center region’’, the ‘‘cell edge region’’, and the ‘‘cell corner region’’ as before. Note that the notion of ‘‘cell’’ is less straightforward than in single-tier networks—it is based on the maximum average signal strength instead of distance only. In other words, it is determined jointly by the power and distance of the BSs.

The definition can include shadowing and load biasing when such factors are relevant. For practical systems, each user measures the average received signal strengths of a list of potential serving BSs in the network. A user is classified to be in  $\mathcal{C}_1$  when it receives a much stronger signal on average from its serving BS than from all the interfering ones; a user within  $\mathcal{C}_2$  receives signals of similar strength from two strongest BSs and much weaker signals from the interfering ones;  $\mathcal{C}_3$  is defined analogously. The cooperation scheme is that a user receiving similar signal strength from  $i$  BSs is jointly served by  $i$  BSs, where  $\gamma$  defines the ‘‘similarity’’.

### B. Homogeneous Independent Poisson Networks

The homogeneous independent Poisson (HIP) model [18, Def. 2] models a  $K$ -tier network  $\Phi = \bigcup_{i=1}^K \Phi_i$ , where BSs of the  $i$ -th tier are modeled using a homogeneous PPP  $\Phi_i \subset \mathbb{R}^2$  with intensity  $\lambda_i$ , is independent of the other tiers, and transmit with power  $P_i$ .

We focus on the typical user at the origin  $o$ . Let  $\Xi = \bigcup_{x \in \Phi} \{\|x\|^\alpha / P_{v(x)}\}$ , we obtain the distance process—a non-homogeneous PPP on  $\mathbb{R}^+$ . Its intensity function is

$$\lambda(t) = \sum_{i=1}^K \lambda_i \pi \delta P_i t^{\delta-1}, \quad t \in \mathbb{R}^+, \quad (40)$$

where  $\delta = 2/\alpha$ . Arranging the elements in  $\Xi$  in ascending order, we have  $\xi_i = \|x_i\|^\alpha / P_{v(x_i)}$  where  $\xi_1 < \xi_2 < \dots$ . Note that  $\xi_i^{-1}$  is the average received signal power from the  $i$ -th strongest BS. The joint distribution of  $\xi_1 < \xi_2 < \xi_3$  is given by [10] as

$$f_{\xi_1, \xi_2, \xi_3}(x, y, z) = (\lambda_{\text{eq}} \pi \delta)^3 \exp(-\lambda_{\text{eq}} \pi z^\delta) (xyz)^{\delta-1}, \quad (41)$$

for  $0 \leq x \leq y \leq z$  and  $\lambda_{\text{eq}} = \sum_{i=1}^K \lambda_i P_i^\delta$ .

For the HIP model, the success probability is independent of the number of network tiers  $K$  and the power level  $P_i$  in each tier [10], so is the meta distribution [21]. The evaluation of the metrics of interest is omitted, since this generalization to multi-tier networks is but a redefinition of the three regions.

## VIII. CONCLUSION

In this paper, we give a mathematical definition of cell regions based on the relative distances of three nearest BSs. The idea of user grouping based on relative received signal strengths generalizes to other channel models and heterogeneous networks. By enabling BS cooperation based on users’ location, users vulnerable to interference can benefit from extra BS resources from nearby BS(s) without harming the network throughput. We quantify the impact of the cooperation level and the path loss exponent from the asymptotic SIR gain, the success probability, the variance of the link success probability as well as the normalized spectral efficiency. We show that a moderate level of BS cooperation is optimal to improve the individual link quality without compromising users’ throughput.

This work permits many extensions. The proposed definition of cell regions can be applied in the scenario of handover where mobile users in the cell corner region can be connected to two or more BSs with similar signal strengths. The framework can be applied to uplink interference management and non-orthogonal multiple access (NOMA) transmission techniques.

## APPENDIX

### A. Proof of Theorem 1

The asymptotic SIR gain  $G$  can be expressed as

$$G = \frac{\text{MISR}_{\text{PPP}}}{\text{MISR}_\gamma}.$$

The MISR of the 1D PPP without cooperation is

$$\text{MISR}_{\text{PPP}} = \sum_{i=2}^{\infty} \mathbb{E} \left[ \left( \frac{r_1}{r_i} \right)^\alpha \right] = \frac{1}{\alpha - 1}, \quad (42)$$

by using  $\mathbb{P}(r_1/r_i \leq x) = 1 - (1 - x)^{i-1}$  [18]. Note that this case can be generalized to  $d$ -D easily:  $\text{MISR}_{\text{PPP}} = d/(\alpha - d) = \delta/(1 - \delta)$  where  $\delta = d/\alpha$ .

We determine  $\text{MISR}_\gamma$  by calculating it for the two regions and adding the results, *i.e.*,

$$\text{MISR}_\gamma = \text{MISR}_{\mathcal{C}_1} + \text{MISR}_{\mathcal{C}_2},$$

where  $\text{MISR}_{\mathcal{C}_i}$  denotes the MISR within  $\mathcal{C}_i$ . For  $\mathcal{C}_1$ , we have

$$\begin{aligned} \text{MISR}_{\mathcal{C}_1} &= \sum_{i>1} \mathbb{E} \left[ \left( \frac{r_1}{r_i} \right)^\alpha \mathbb{1}_{\mathcal{C}_1} \right] \\ &\stackrel{(a)}{=} \mathbb{E} \left[ \left( \frac{r_1}{r_2} \right)^\alpha \mathbb{1}_{\mathcal{C}_1} \right] \sum_{i>1} \mathbb{E} \left[ \left( \frac{r_2}{r_i} \right)^\alpha \right] \\ &\stackrel{(b)}{=} \mathbb{E} \left[ \left( \frac{r_1}{r_2} \right)^\alpha \mathbb{1}_{\mathcal{C}_1} \right] \frac{\alpha + 1}{\alpha - 1}, \end{aligned} \quad (43)$$

where  $\mathbb{1}_{\mathcal{C}_i}$  is the indicator function that the typical user falls into  $\mathcal{C}_i$ . Step (a) follows from the fact that only the first term in  $\text{MISR}_{\mathcal{C}_1}$  is constrained by the cooperation region, which can be calculated using the joint distribution of  $r_1$  and  $r_2$ . Step (b) follows from the relative distance process calculation in [22].

Similarly, we obtain the MISR in  $\mathcal{C}_2$  as

$$\text{MISR}_{\mathcal{C}_2} = \mathbb{E} \left[ \frac{1}{1 + (r_2/r_1)^\alpha} \mathbb{1}_{\mathcal{C}_2} \right] \frac{2}{\alpha - 1}. \quad (44)$$

Combining (42), (43) and (44) we can write

$$\begin{aligned} G &= \frac{1}{(\alpha + 1) \mathbb{E} \left[ \left( \frac{r_1}{r_2} \right)^\alpha \mathbb{1}_{\mathcal{C}_1} \right] + 2 \mathbb{E} \left[ \frac{1}{1 + (r_2/r_1)^\alpha} \mathbb{1}_{\mathcal{C}_2} \right]} \\ &= \left( \rho^{1+\alpha} + 2 \int_0^\infty \int_x^\infty \frac{\exp(-y)}{1 + (\frac{y}{x})^\alpha} dy dx \right)^{-1} \\ &\stackrel{(a)}{=} \left( \rho^{1+\alpha} + 2 \left( 1 - \rho - \int_\rho^1 \frac{1}{1 + z^\alpha} dz \right) \right)^{-1}. \end{aligned}$$

Step (a) follows from the change of variable  $z = x/y$ .

### B. Proof of Proposition 1

$$M_b = \mathbb{E}[P_s(\theta)^b] = \sum_{i=1}^2 \mathbb{E}[P_s(\theta)^b \mathbb{1}_{\mathcal{C}_i}].$$

where  $\mathbb{1}_{\mathcal{C}_i}$  is the indicator function that is one when  $o \in \mathcal{C}_i$  and zero otherwise.

We know that  $\mathbb{E}[P_s(\theta)^b \mathbb{1}_{\mathcal{C}_1}] = \rho/2 F_1(b, -\delta; 1 - \delta; -\rho^\alpha \theta)$  from [3]. For  $\mathcal{C}_2$ ,

$$\begin{aligned} &\mathbb{E}[P_s(\theta)^b \mathbb{1}_{\mathcal{C}_2}] \\ &\stackrel{(a)}{=} \int_0^\infty \int_x^\infty \exp \left( -y - \int_y^\infty 1 - \frac{1}{(1 + st^{-\frac{1}{\delta}})^b} dt \right) dy dx \\ &\stackrel{(b)}{=} \int_0^\infty \int_{\frac{x}{y^{\frac{1}{\delta}}}}^\infty \exp \left( -y - \int_{\frac{1}{y^{\frac{1}{\delta}}}}^\infty \left( 1 - \frac{1}{(1 + su^{-1})^b} \right) u^{\delta-1} \delta du \right) dy dx \\ &= \int_0^\infty \int_x^\infty \exp \left( -y {}_2F_1 \left( b, -\delta; 1 - \delta; -\frac{\theta}{1 + (\frac{y}{x})^{\frac{1}{\delta}}} \right) \right) dy dx \\ &\stackrel{(c)}{=} \int_1^{\frac{1}{\rho}} \frac{1}{(t {}_2F_1(b, -\delta, 1 - \delta, -\theta/(1 + t^{\frac{1}{\delta}})))^2} dt. \end{aligned}$$

Step (a) follows from letting  $s = \theta/(x^{-\alpha} + y^{-\alpha})$  and using the probability generating functional (PGFL) of the PPP [23]. Step (b) follows from  $u = t^{1/\delta}$  and  $\int_r^\infty (1 - 1/(1 + sx^{-1})^b) x^{\delta-1} dx = r^\delta (-1 + {}_2F_1(b, -\delta, 1 - \delta, -s/r))/\delta$ . Step (c) follows from  $t = y/x$ .

### C. Proof of Theorem 2

The asymptotic SIR gain  $G$  can be expressed as

$$G = \frac{\text{MISR}_{\text{PPP}}}{\text{MISR}_\gamma}.$$

The MISR of the 2D PPP without cooperation is  $\text{MISR}_{\text{PPP}} = 2/(\alpha - 2)$  [18], and

$$\text{MISR}_\gamma = \text{MISR}_{\mathcal{C}_1} + \text{MISR}_{\mathcal{C}_2} + \text{MISR}_{\mathcal{C}_3},$$

where  $\text{MISR}_{\mathcal{C}_i}$  denotes the MISR within  $\mathcal{C}_i$ . For  $\mathcal{C}_1$ , we have

$$\begin{aligned} \text{MISR}_{\mathcal{C}_1} &= \sum_{i>1} \mathbb{E} \left[ \left( \frac{r_1}{r_i} \right)^\alpha \mathbb{1}_{\mathcal{C}_1} \right] \\ &\stackrel{(a)}{=} \mathbb{E} \left[ \left( \frac{r_1}{r_2} \right)^\alpha \mathbb{1}_{\mathcal{C}_1} \right] \sum_{i>1} \mathbb{E} \left[ \left( \frac{r_2}{r_i} \right)^\alpha \right], \end{aligned}$$

where step (a) follows from the fact that only the first term in  $\text{MISR}_{\mathcal{C}_1}$  depends on the cooperation region. It can be calculated using the joint distribution of  $r_1$  and  $r_2$  as

$$\mathbb{E} \left[ \left( \frac{r_1}{r_2} \right)^\alpha \mathbb{1}_{\mathcal{C}_1} \right] = \int_0^\infty \int_{\frac{x}{\rho}}^\infty f_{r_1, r_2}(x, y) \left( \frac{r_1}{r_2} \right)^\alpha dy dx.$$

The second term can be calculated by considering the relative distance process [22]

$$\sum_{i>1} \mathbb{E} \left[ \left( \frac{r_2}{r_i} \right)^\alpha \right] = 1 + \frac{4}{\alpha - 2}.$$

Similarly, we obtain the MISR in  $\mathcal{C}_2$  and  $\mathcal{C}_3$  as

$$\begin{aligned} \text{MISR}_{\mathcal{C}_2} &= \sum_{i>2} \mathbb{E} \left[ \frac{r_i^{-\alpha}}{r_1^{-\alpha} + r_2^{-\alpha}} \mathbb{1}_{\mathcal{C}_2} \right] \\ &= \mathbb{E} \left[ \frac{(r_1/r_3)^\alpha}{1 + (r_1/r_2)^\alpha} \mathbb{1}_{\mathcal{C}_2} \right] \sum_{i>2} \mathbb{E} \left[ \left( \frac{r_3}{r_i} \right)^\alpha \right], \end{aligned}$$

where

$$\sum_{i>2} \mathbb{E} \left[ \left( \frac{r_3}{r_i} \right)^\alpha \right] = 1 + \frac{6}{\alpha - 2},$$

and

$$\begin{aligned} \text{MISR}_{\mathcal{C}_3} &= \sum_{i>3} \mathbb{E} \left[ \frac{r_i^{-\alpha}}{r_1^{-\alpha} + r_2^{-\alpha} + r_3^{-\alpha}} \mathbb{1}_{\mathcal{C}_3} \right] \\ &= \mathbb{E} \left[ \frac{(r_1/r_3)^\alpha}{1 + (r_1/r_2)^\alpha + (r_1/r_3)^\alpha} \mathbb{1}_{\mathcal{C}_3} \right] \sum_{i>3} \mathbb{E} \left[ \left( \frac{r_3}{r_i} \right)^\alpha \right], \end{aligned}$$

where

$$\sum_{i>3} \mathbb{E} \left[ \left( \frac{r_3}{r_i} \right)^\alpha \right] = \frac{6}{\alpha - 2}.$$

## REFERENCES

- [1] K. Feng and M. Haenggi, "A tunable base station cooperation scheme for Poisson cellular networks," in *2018 52nd Annual Conference on Information Sciences and Systems (CISS)*, Mar 2018.
- [2] D. Gesbert, S. Hanly, H. Huang, S. S. Shitz, O. Simeone, and W. Yu, "Multi-cell MIMO cooperative networks: A new look at interference," *IEEE Journal on Selected Areas in Communications*, vol. 28, no. 9, pp. 1380–1408, Dec 2010.
- [3] K. Feng and M. Haenggi, "On the location-dependent SIR gain in cellular networks," *IEEE Wireless Communications Letters*, pp. 1–1, Jan 2019 (Early Access).
- [4] S. Y. Jung, H. Lee, and S. Kim, "Worst-case user analysis in Poisson Voronoi cells," *IEEE Communications Letters*, vol. 17, no. 8, pp. 1580–1583, August 2013.
- [5] R. Irmer, H. Droste, P. Marsch, M. Grieger, G. Fettweis, S. Brueck, H.-P. Mayer, L. Thiele, and V. Jungnickel, "Coordinated multipoint: Concepts, performance, and field trial results," *IEEE Communications Magazine*, vol. 49, pp. 102–111, Feb 2011.
- [6] V. Kotsch and G. Fettweis, "On synchronization requirements and performance limitations for CoMP systems in large cells," in *2011 8th International Workshop on Multi-Carrier Systems Solutions*, May 2011, pp. 1–5.
- [7] J. Yoon and G. Hwang, "Distance-based inter-cell interference coordination in small cell networks: Stochastic geometry modeling and analysis," *IEEE Transactions on Wireless Communications*, vol. 17, no. 6, pp. 4089–4103, Jun 2018.
- [8] F. Baccelli and A. Giovanidis, "A stochastic geometry framework for analyzing pairwise-cooperative cellular networks," *IEEE Transactions on Wireless Communications*, vol. 14, no. 2, pp. 794–808, Feb 2015.
- [9] R. Tanbourgi, S. Singh, J. G. Andrews, and F. K. Jondral, "A tractable model for noncoherent joint-transmission base station cooperation," *IEEE Transactions on Wireless Communications*, vol. 13, no. 9, pp. 4959–4973, Sept 2014.
- [10] G. Nigam, P. Minero, and M. Haenggi, "Coordinated multipoint joint transmission in heterogeneous networks," *IEEE Transactions on Communications*, vol. 62, no. 11, pp. 4134–4146, Nov 2014.
- [11] Q. Cui, X. Yu, Y. Wang, and M. Haenggi, "The SIR meta distribution in Poisson cellular networks with base station cooperation," *IEEE Transactions on Communications*, vol. 66, no. 3, pp. 1234–1249, Mar 2018.
- [12] A. H. Sakr and E. Hossain, "Location-aware cross-tier coordinated multipoint transmission in two-tier cellular networks," *IEEE Transactions on Wireless Communications*, vol. 13, no. 11, pp. 6311–6325, Nov 2014.
- [13] N. Ross and D. Schuhmacher, "Wireless network signals with moderately correlated shadowing still appear Poisson," *IEEE Transactions on Information Theory*, vol. 63, no. 2, pp. 1177–1198, Feb 2017.
- [14] B. Błaszczyszyn, P. Mühlthaler, and Y. Toor, "Stochastic analysis of Aloha in vehicular ad hoc networks," *Annals of Telecommunications*, vol. 68, pp. 95–106, Feb 2013.
- [15] J. G. Andrews, F. Baccelli, and R. K. Ganti, "A tractable approach to coverage and rate in cellular networks," *IEEE Transactions on Communications*, vol. 59, no. 11, pp. 3122–3134, Nov 2011.
- [16] M. Haenggi, "The meta distribution of the SIR in Poisson bipolar and cellular networks," *IEEE Transactions on Wireless Communications*, vol. 15, no. 4, pp. 2577–2589, Apr 2016.
- [17] X. Zhang and M. Haenggi, "A stochastic geometry analysis of inter-cell interference coordination and intra-cell diversity," *IEEE Transactions on Wireless Communications*, vol. 13, no. 12, pp. 6655–6669, Dec 2014.
- [18] M. Haenggi, "The mean interference-to-signal ratio and its key role in cellular and amorphous networks," *IEEE Wireless Communications Letters*, vol. 3, no. 6, pp. 597–600, Dec 2014.
- [19] —, "Efficient calculation of meta distributions and the performance of user percentiles," *IEEE Wireless Communications Letters*, vol. 7, no. 6, pp. 982–985, Dec 2018.
- [20] S. Guruacharya and E. Hossain, "Approximation of meta distribution and its moments for Poisson cellular networks," *IEEE Wireless Communications Letters*, vol. 7, no. 6, pp. 1074–1077, Dec 2018.
- [21] Y. Wang, M. Haenggi, and Z. Tan, "SIR meta distribution of  $K$ -tier downlink heterogeneous cellular networks with cell range expansion," *IEEE Transactions on Communications*, vol. 67, no. 4, pp. 3069–3081, April 2019.
- [22] R. K. Ganti and M. Haenggi, "Asymptotics and approximation of the SIR distribution in general cellular networks," *IEEE Transactions on Wireless Communications*, vol. 15, no. 3, pp. 2130–2143, Mar 2016.
- [23] M. Haenggi, *Stochastic geometry for wireless networks*. Cambridge University Press, 2012.



**Ke Feng** (S'19) received the B. Eng. in information engineering from the University of Science and Technology of China (USTC), Hefei, China, in 2016 and the M.S. degree in electrical engineering from the University of Notre Dame, Notre Dame, IN, USA, in 2019, where she is currently working towards her Ph.D. degree. She held an internship position at Huawei US R&D in Bridgewater, NJ, in 2018. Ke's research interests lie in wireless network modelling and analysis, information theory and graph theory.



**Martin Haenggi** (S'95-M'99-SM'04-F'14) received the Dipl.-Ing. (M.Sc.) and Dr.sc.techn. (Ph.D.) degrees in electrical engineering from the Swiss Federal Institute of Technology in Zurich (ETH) in 1995 and 1999, respectively. Currently he is the Freimann Professor of Electrical Engineering and a Concurrent Professor of Applied and Computational Mathematics and Statistics at the University of Notre Dame, Indiana, USA. In 2007–2008, he was a visiting professor at the University of California at San Diego, and in 2014–2015 he was an Invited Professor at EPFL, Switzerland. He is a co-author of the monographs "Interference in Large Wireless Networks" (NOW Publishers, 2009) and "Stochastic Geometry Analysis of Cellular Networks" (Cambridge University Press, 2018) and the author of the textbook "Stochastic Geometry for Wireless Networks" (Cambridge, 2012), and he published 15 single-author journal articles. His scientific interests lie in networking and wireless communications, with an emphasis on cellular, amorphous, ad hoc (including D2D and M2M), cognitive, and vehicular networks. He served as an Associate Editor of the Elsevier Journal of Ad Hoc Networks, the IEEE Transactions on Mobile Computing (TMC), the ACM Transactions on Sensor Networks, as a Guest Editor for the IEEE Journal on Selected Areas in Communications, the IEEE Transactions on Vehicular Technology, and the EURASIP Journal on Wireless Communications and Networking, as a Steering Committee member of the TMC, and as the Chair of the Executive Editorial Committee of the IEEE Transactions on Wireless Communications (TWC). From 2017 to 2018, he was the Editor-in-Chief of the TWC. He also served as a Distinguished Lecturer for the IEEE Circuits and Systems Society, as a TPC Co-chair of the Communication Theory Symposium of the 2012 IEEE International Conference on Communications (ICC'12), of the 2014 International Conference on Wireless Communications and Signal Processing (WCSP'14), and the 2016 International Symposium on Wireless Personal Multimedia Communications (WPMC'16). For both his M.Sc. and Ph.D. theses, he was awarded the ETH medal. He also received a CAREER award from the U.S. National Science Foundation in 2005 and three awards from the IEEE Communications Society, the 2010 Best Tutorial Paper award, the 2017 Stephen O. Rice Prize paper award, and the 2017 Best Survey paper award, and he is a 2017 and 2018 Clarivate Analytics Highly Cited Researcher.